INSTITUTE OF PHYSICS PUBLISHING JOURNAL OF PHYSICS D: APPLIED PHYSICS
J. Phys. D: Appl. Phys. **34** (2001) 3097–3108 PII: S0022-3727(01)27014-4

Resistivity of polycrystalline zinc oxide films: current status and physical limit

K Ellmer

Hahn-Meitner-Institut, Department of Solare Energetik, D-14109 Berlin, Glienicker Strasse 100, Germany

E-mail: ellmer@hmi.de

Received 23 July 2001
Published 23 October 2001
Online at stacks.iop.org/JPhysD/34/3097

Abstract

Heavily doped zinc oxide films are used as transparent and conductive electrodes, especially in thin film solar cells. Despite decades of research on zinc oxide it is not yet clear what the lower limit of the resistivity of such films is. Therefore, the electrical parameters of zinc oxide films deposited by magnetron sputtering, metal organic chemical vapour deposition and pulsed laser ablation are reviewed and related to the deposition parameters. It is found that the lowest resistivities are in the range of 1.4 to 2×10^{-4} Ω cm, independently of the deposition method. The highest reported Hall mobilities are about 60 $cm^2\ V^{-1}\ s^{-1}$. The thin film electrical data are compared with the corresponding values of single crystalline zinc oxide and with that of boron and phosphorous doped crystalline silicon. From this comparison it can be seen that the dependence of the Hall mobilities on the carrier concentration n are quite similar for silicon and zinc oxide. In the region $n > 5 \times 10^{20}$ cm^{-3}, which is most important for the application of zinc oxide as a transparent and conductive electrode, phosphorous doped silicon has a mobility only slightly higher than zinc oxide. The experimental data on the electron and hole mobilities in silicon as a function of the impurity concentration have been described by a fit function (Masetti *et al* 1983), which can also be applied with different fitting parameters to the available zinc oxide mobility data. A comparison of the experimental data with the well known ionized impurity scattering theories of Conwell–Weisskopf (1946) and Brooks–Herring–Dingle (1955) shows that these theories are not able to describe the data very well, even if the non-parabolic band structure is taken into account. As in the case of silicon, an additional reduction of the mobility also occurs for zinc oxide for concentrations $n > 5 \times 10^{20}$ cm^{-3}, which can be ascribed qualitatively to the clustering of charge carriers connected with increased scattering due to the Z^{-2} dependence of the scattering cross section on the charge Z of the scattering centre. The presented review of the charge carrier transport in zinc oxide indicates that a physical limit due to ionized impurity scattering is reached for homogeneously doped layers. Due to the universal nature of this limitation it is suggested that it also applies to the other important materials indium–tin (ITO) and tin oxide. Experiments are proposed to overcome this limit.

1. Introduction

Zinc oxide (ZnO) belongs to the class of transparent conductive oxides (TCO) like the compound semiconductors indium oxide (In_2O_3) and tin oxide (SnO_2) [1]. These materials possess a wide energy bandgap ($E_g > 3.4$ eV) and are therefore transparent in the wavelength region from about 350 to >800 nm, where the long wavelength cutoff depends on the

charge carrier concentration. TCO films can be prepared with resistivities in the region of 1 to 5×10^{-4} Ω cm, only one to two orders of magnitude higher than typical metals ($\rho_{Cu} = 1.7\,\mu\Omega\,\text{cm}$, $\rho_{Mo} = 5.4\,\mu\Omega\,\text{cm}$, $\rho_{Pb} = 21\,\mu\Omega\,\text{cm}$). This makes these materials very well suited for transparent electrodes in flat panel displays (liquid crystal, electroluminescence and plasma displays), thin film solar cells, microwave oven windows, low emissivity glass, thermal solar collectors, etc. In the last few years zinc oxide has gained increasing attention as a TCO material because of the higher abundance compared to the other TCO materials (about a factor of 1000 more abundant than indium, see table 2 later). Another advantage of zinc oxide is its stability in hydrogen containing atmospheres [2], e.g., in a silan (SiH_4) plasma discharge, which is used for the preparation of a-Si:H thin film solar cells [3]. Recently, zinc oxide single crystals [4] of high quality have been prepared. Such crystals are promising candidates as substrates for gallium nitride epitaxial films for blue laser applications. Moreover, zinc oxide itself has been investigated as a material for blue lasers due to its direct bandgap [5, 6].

Until now the research in the field of TCO films has been performed on an empirical basis, which is not surprising taking into account that the doping mechanism even in single crystalline zinc oxide (and other TCO materials) is not yet clear [7]. Also the theoretical understanding of other heavily doped semiconductors, even silicon, is poor [8, 9]. In view of the fact, that the resistivities of TCO films have reached a limit around 10^{-4} Ω cm, attempts have been made in the last five years to develop new ternary TCO materials [10–12] in order to surmount this limit.

As typical representatives of compound semiconductors these oxides can be made conductive by intrinsic (defects) or extrinsic (dopants) charge carriers. If thin films of zinc oxide are prepared intrinsically, i.e. without intrinsic or extrinsic dopants their resistivity is very high: of the order of 1500 Ω cm perpendicular to and $>10^9$ Ω cm parallel to the substrate [13]. The high value parallel to the substrate is due to the hindered carrier transport across the grain barriers. For comparison, the intrinsic zinc oxide single crystals have typical resistivities in the range of 1–10 Ω cm [4, 14]. However, Kobiakov [15] reported dark resistivities of up to $\approx 10^{12}$ Ω cm for ZnO crystal lithium compensated by annealing at 1070 K in a Li_2CO_3 melt.

The low resistivity at room temperature which is required for the application of TCO films as transparent electrodes can be achieved in two ways:

- creation of intrinsic donors by lattice defects (for instance oxygen vacancies or metal atoms on interstitial lattice sites) or
- introduction of extrinsic dopants (either metals with oxidation number three on substitutional metal lattice sites or halogens with oxidation number minus one on oxygen lattice sites).

The first possibility can be realized during the deposition by carefully adjusting the oxygen partial pressure and deposition rate. The other way is a reduction process of the oxide after deposition, for instance by annealing in vacuum or in a hydrogen containing atmosphere [16]. However, it has been found that such films exhibit properties, which are not well suited for application. First, the resistivity is only about 10^{-2} to 10^{-3} Ω cm. Furthermore, these films are not stable at ambient conditions (especially at higher temperatures) due to the reoxidation of the oxygen deficient films.

Therefore, in most cases extrinsic dopants are added during the deposition. In reality in doped oxide films both doping mechanisms occur simultaneously. By increasing the oxygen partial pressure during (or after) preparation the dopants become oxidized and hence lose its doping effect. Another complication arises due to the variation of phases, structure and morphology when changing the deposition parameters, especially the oxygen partial pressure. Actually, ZnO films (as well as other TCO films) are phase mixtures containing not only the desired phase (e.g., ZnO) but also secondary phases, like $ZnAl_2O_4$ (gahnite), Al_2O_3 (alumina) or ZnO_2, a low temperature phase in the Zn–O system. Normally, these additional phases which of course contribute to the electronic and structural–mechanical film properties, are not detected by standard analytical techniques like x-ray diffraction and photoelectron spectroscopy due to their low concentrations. Only recently these phases were identified in aluminium-doped zinc oxide by transmission electron microscopy (TEM) and selected area electron diffraction (SAD) [17]. Minami [11] reported the doping of zinc oxide by adding elements like Y, Zr, Ti and Hf, which do not exhibit an additional valence electron like the more common dopants B, Al, Ga or In. Nevertheless, Minami obtained resistivities in the low 10^{-4} Ω cm range. This observation is somewhat puzzling with respect to the conventional explanation of extrinsic doping (see above). However, by assuming that these oxide forming additives could attract oxygen from the zinc oxide lattice, thus generating oxygen vacancies, the doping would be actually caused by oxygen vacancies.

Concerning the application of zinc oxide and other TCO materials as transparent electrodes in displays and thin film solar cells the question arises, what the lower limit of the resistivity of such degenerate semiconducting thin films is. The well known reviews about TCO materials [1, 11, 12, 18] do not address the physical limits of the resistivity. Bellingham *et al* [19] applied the ionized impurity scattering model of Brooks and Herring [20], Dingle [21] and Moore [22] to TCO films. They came to the conclusion that ionized impurities govern the transport for carrier densities above 10^{19} cm^{-3}. Bellingham *et al* [19] estimated a limiting carrier mobility of 90 cm^2 V^{-1} s^{-1} for the three mentioned TCO materials. Minami *et al* [11, 23] combined scattering at grain boundaries and ionized impurity scattering to explain their results on self-doped and extrinsically (B, Al, Ga) doped ZnO films. In the region $n > 10^{20}$ cm^{-3} the experimental data could be described only by taking into account a very strong non-parabolicity of the zinc oxide conduction band. With respect to the theoretical scattering models, it is not really clear which charge state of the dopant has to be used in the calculations. For extrinsic dopants on cation lattice places, the charge state should be $Z = 1$, while oxygen vacancies exhibit a charge state $Z = 2$, leading to lower mobilities.

It is the aim of this paper to review the electrical parameters of doped and undoped zinc oxide and its dependence on such important deposition parameters as substrate temperature and sputtering pressure. The dependence of the mobility on the charge carrier concentration is compared with existing

analytical models for charge carrier scattering in heavily doped semiconductors.

This paper is organized in the following way: section 2.1 summarizes the reported electrical properties of ZnO films, focusing on sputter deposited films. For comparison also films prepared by metal organic chemical vapour deposition (MOCVD) and pulsed laser ablation deposition (PLD) have been included. In section 2.2 the thin film data are compared with the available electrical parameters of doped and undoped ZnO single crystals and with the mobilities of the most advanced semiconductor silicon. The experimental data are compared with the well known analytical models for ionized impurity scattering in section 2.3. Furthermore, a semiempirical fit formula of Masetti *et al* [24] (see also Klaassen [25]), developed for the charge carrier mobility dependence of silicon is applied to zinc oxide. In the conclusions (section 3) a physical limit for transparent and conductive ZnO films is estimated. A proposal for surmounting this limit is given section 4.

2. Electrical properties

2.1. Experimental data of ZnO films

In the following literature resistivity and mobility data (room temperature measurements) are compiled for zinc oxide films deposited by different methods:

- reactive and non-reactive magnetron sputtering,
- metalorganic chemical vapour deposition (MOCVD) and
- pulsed laser ablation deposition (PLD).

Emphasis is given to films prepared by magnetron sputtering, a technique that is already widely used both in research and industry [26]. Figures 1(a)–(d) show a collection of resistivity and Hall mobility data for polycrystalline zinc oxide films versus the substrate temperature and the sputtering pressure (in the case of magnetron sputtered films). Part of these data were presented in a recent paper [27]. The data for sputter deposited films were taken from [11, 28–51], the data for MOCVD-deposited films from [52–59] and those for PLD-prepared films are from [60, 61].

The lowest resistivity values reported are about $2 \times 10^{-4}\ \Omega$ cm [29, 50], apart from two values of $1.4 \times 10^{-4}\ \Omega$ cm for an heteroepitaxially sputtered ZnO film and a PLD film. Most of the electrical measurements of heavily doped ($>10^{19}$ cm^{-3}) zinc oxide were obtained for polycrystalline thin films. Data on heavily doped single crystals or epitaxial layers are rare [62, 63]. The scattering of the resistivity and mobility data is large. The dopants used for the ZnO films: Al, B, Ga, In and Sn lead to comparable resistivities of the zinc oxide films [30]. However, aluminium is the dopant mostly used. As can be seen from figures 1(a) and (b), the resistivity data do not exhibit a correlation with the substrate temperature T_{sub}, while the mobility values tentatively show an increase with T_{sub}, which is understandable because of the better crystalline quality of films prepared at higher substrate temperatures. In data series of the same research group the beneficial effect of an increased substrate temperature can be seen more clearly (see for instance Minami *et al* [64]). When comparing the different deposition methods one has to keep in mind that the growth is governed by different microscopic processes.

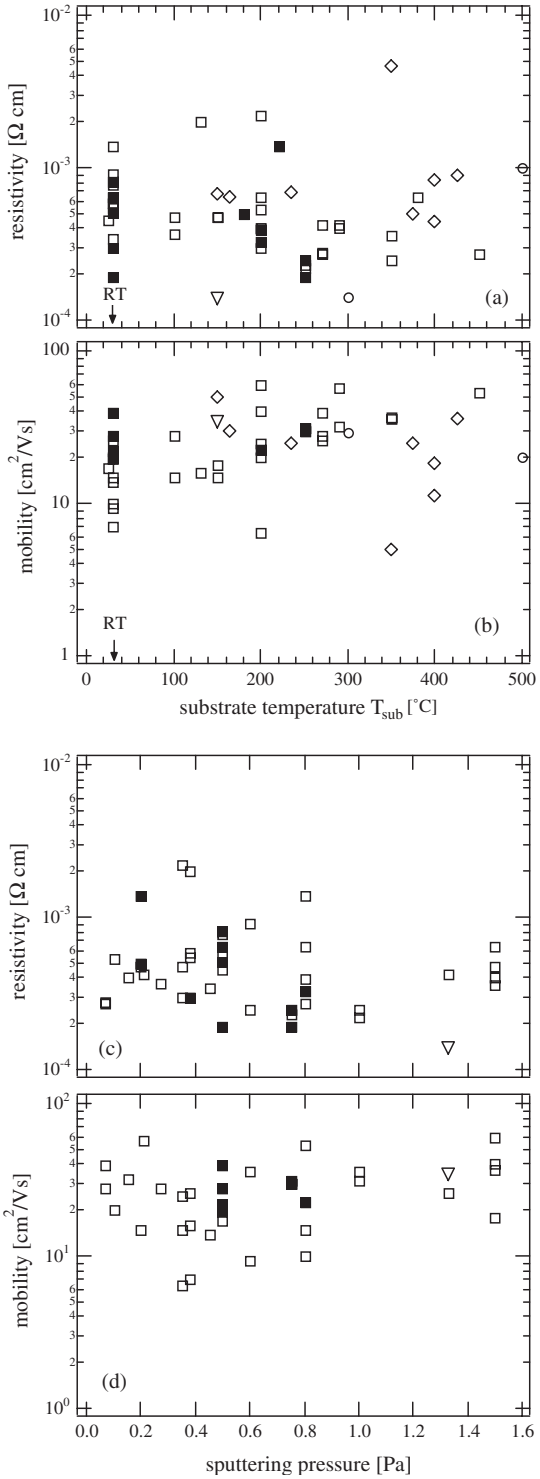

Figure 1. The dependence of the resistivity (a) and (c) and Hall mobility (b) and (d) of doped ZnO layers on the substrate temperature (a) and (b) and on the sputtering pressure (c) and (d). The full symbols denote layers which were prepared on substrates positioned perpendicular to the sputtering target. The point marked by a triangle belongs to an epitaxial ZnO film. The films were deposited by magnetron sputtering (■, □, ▽), MOCVD (◇) and pulsed laser deposition (○). RT is room temperature.

While MOCVD and PLD rely on a pure thermal activation of the growth process, magnetron sputtering is characterized—

as is every plasma assisted process—by an additional energy input from the plasma into the growing film. Therefore, lower growth temperatures are possible in magnetron sputtering deposition, which is also visible from figures 1(a) and (b). The fact, that the resistivity is independent of such important experimental parameters like the substrate temperature (and total sputtering pressure) as depicted in figure 1 is certainly due to differences in the sputtering configurations of different groups (which are not always reported). Parameters like target-to-substrate distance, type of the used magnetron sputtering source (balanced or unbalanced magnetic field), deposition rate, arrangement of the substrate relative to the target (parallel or perpendicular) have a strong influence on the film properties. For example, the full symbols in figure 1 mark the electronic parameters of ZnO films, which were deposited onto substrates arranged perpendicularly relative to the target. This deposition configuration is characterized by a low deposition rate, a high ion-to-neutral ratio and reduces the bombardment of the films by species with high energies (reflected argon atoms or negative oxygen ions), thus leading to low resistivities even for room temperature deposition [65, 66].

Obviously, the ion assistance of the film growth during magnetron sputtering allows the deposition of zinc oxide films with a high crystallographic and electronic quality even at room temperature [27, 67]. The effects of the ion assisted growth depend significantly on the energy of the species that influence the growth process and on the ion-to-neutral ratio during the film growth. The dependence of ρ and μ on the sputtering pressure (figures 1(c) and (d)) does not show a clear trend, which could have been expected due to the variation of the particle energies at the growing film with sputtering pressure.

Zinc oxide films have been prepared now for more than twenty years with different deposition methods and a lot of technological effort has been put into this research. Therefore, it is interesting to look for a trend of the electrical data of the ZnO films over the time (figure 2). Surprisingly, since about 1985 the reported resistivity and mobility values have not changed significantly, despite the fact that a large number of groups have been working in this field. This suggests that there probably exists a physical limitation which prevents reaching resistivities lower than about 1×10^{-4} Ω cm and mobilities larger than about 40 cm^2 V^{-1} s^{-1}. This result is in qualitative agreement with a presentation of Minami [11] of TCO-resistivity data over time. While Minami, in agreement with our assumption, suggests a lower resistivity limit of 1×10^{-4} Ω cm for tin-doped indium oxide (ITO) films, he supposes by a freely drawn line, that ZnO could reach resistivities below 1×10^{-4} Ω cm beyond the year 2000 (see his figure 1). This will be discussed in more detail in section 2.3.

Figure 3 shows the resistivities and Hall mobilities of zinc oxide films as a function of the charge carrier concentration n. As expected, the resistivity decreases with increasing carrier concentration. The Hall mobilities of the heavily doped zinc oxide films show a large scattering and are in the range of 5 to 60 cm^2 V^{-1} s^{-1} with a trend to decrease both with increasing as well as decreasing carrier concentration. The highest reported carrier concentrations are about 1.5×10^{21} cm^{-3}. This corresponds to a dopant concentration of 3.6 at% relative to zinc atoms, though the impurity concentration is often significantly higher. Obviously, higher carrier concentrations are not possible due to a limited solubility of the donor substance in zinc oxide. A comparable observation was

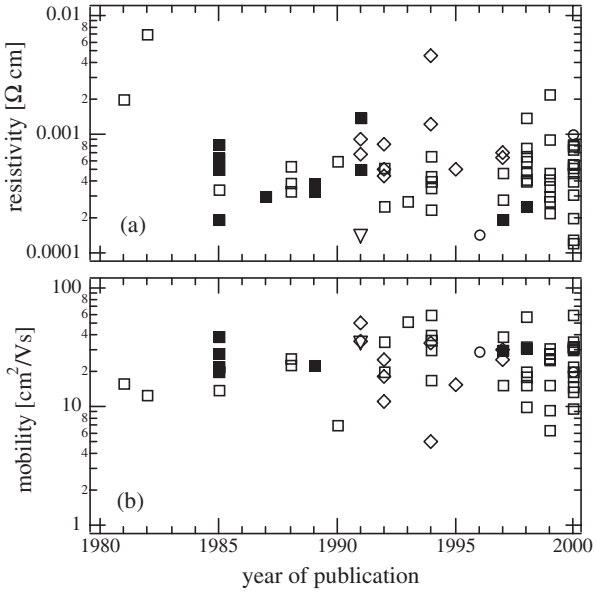

Figure 2. The resistivity (a) and Hall mobility (b) of doped ZnO layers versus the year of publication. The symbols have the same meaning as in figure 1.

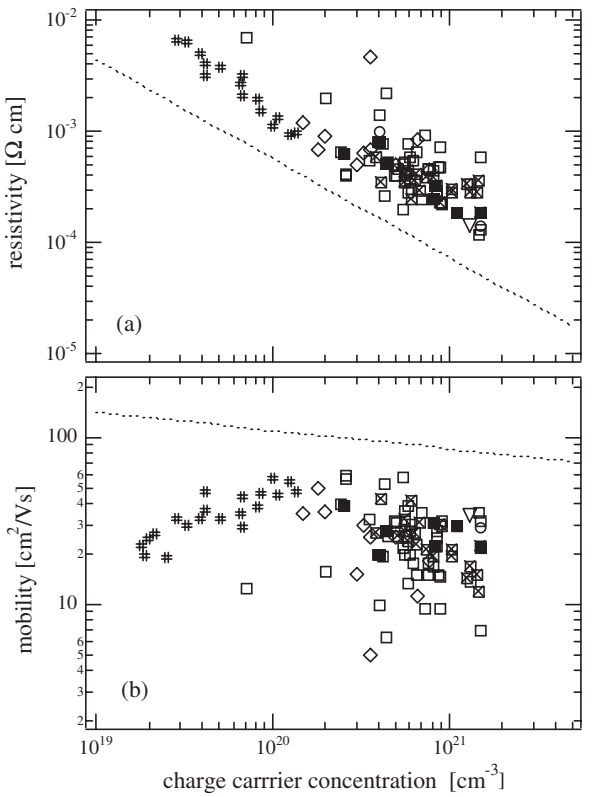

Figure 3. The dependence of the resistivity (a) and Hall mobility (b) of doped and undoped ZnO films on the charge carrier concentration. The symbols have the same meaning as in figure 1. The new symbols denote zinc oxide films without extrinsic dopants (#) and aluminium-doped ZnO films (⊠), both reported by Minami *et al* [23]. The broken curves are theoretical curves, calculated by Bellingham *et al* [19].

reported for tin-doped indium oxide [68], where the maximum carrier concentration (also 1.5×10^{21} cm^{-3}) corresponds to 5 at% of the cation (indium) sites in In_2O_3, while the tin solubility is about 6 at%. For comparison, the solubilities of the well known dopants in silicon are in the same range, for instance 1.5×10^{21} cm^{-3} for phosphorous and 2×10^{21} cm^{-3} for arsenic [69].

The mobility data for oxygen vacancy doped ZnO films of Minami [23] (symbol #) with carrier concentrations from 10^{19} to 10^{20} cm^{-3} decrease with decreasing n. This behaviour is different from that at higher carrier concentrations and is discussed in more detail in section 2.2. The dashed lines in figure 3(a) and (b) are theoretical estimates of Bellingham *et al* [19], based on Dingle's theory [21]. Obviously, the resistivities of the zinc oxide films are underestimated due to a too high mobility. Also the decreasing trend of the mobility versus the carrier concentration n is too weak compared to the experimental data, especially for $n > 5 \times 10^{20}$ cm^{-3}.

2.2. Comparison with data of single crystals

To get a more comprehensive picture of the carrier transport in zinc oxide the resistivity and mobility data have been displayed in figure 4 over a broader range of carrier concentrations. Here, data for doped and undoped single crystalline ZnO (taken from references [4, 62, 70–75]) have been added to the data of figure 3. Now, clearer trends for resistivity and mobility can be observed. The resistivity decreases continuously down to about $n = 5 \times 10^{20}$ cm^{-3}, where it seems to saturate. The mobilities show a significant scattering especially at carrier concentrations above 10^{20} cm^{-3}, where the data belong exclusively to thin polycrystalline films.

While the single crystalline and polycrystalline data merge into a common curve for $n > 1 \times 10^{20}$ cm^{-3}, at lower n values a splitting of the single crystalline and polycrystalline mobility data can be observed. Obviously, this is due to the grain barrier limited transport in polycrystalline thin films, described for instance by Seto [76] for phosphorous-doped silicon films or Bruneaux *et al* [77] for fluorine-doped tin dioxide films. For charge carrier concentrations above about 1×10^{20} cm^{-3} the grain barriers are narrow enough so that the electrons are able to tunnel through the barriers. This means, that the carrier scattering is no longer limited by the grain barriers but is determined by scattering at ionized impurities. Therefore, in this region the polycrystalline thin film values can be compared with the single crystalline data.

The maximum Hall mobilities of lowly doped ZnO single crystals are about 200 cm^2 V^{-1} s^{-1}, limited by scattering at polar-optical phonons [4, 14]. The lowest carrier concentrations reported for undoped zinc oxide crystals are about 1×10^{14} cm^{-3} [73], which seems to be due to intrinsic defects due to stoichiometric deviations in the crystals. It is interesting to note, that the highest resistivities and mobilities have been constant for decades also for the undoped ZnO crystals [4, 62, 70, 73, 78].

Comparing the ZnO mobility data with the theoretical estimation of Bellingham *et al* [19] (broken curves) it can be seen, that the overestimation, already mentioned in section 2.1 is also valid for the single crystal ZnO data.

It is interesting to compare the ZnO mobility data with that of heavily doped single crystalline silicon, the best

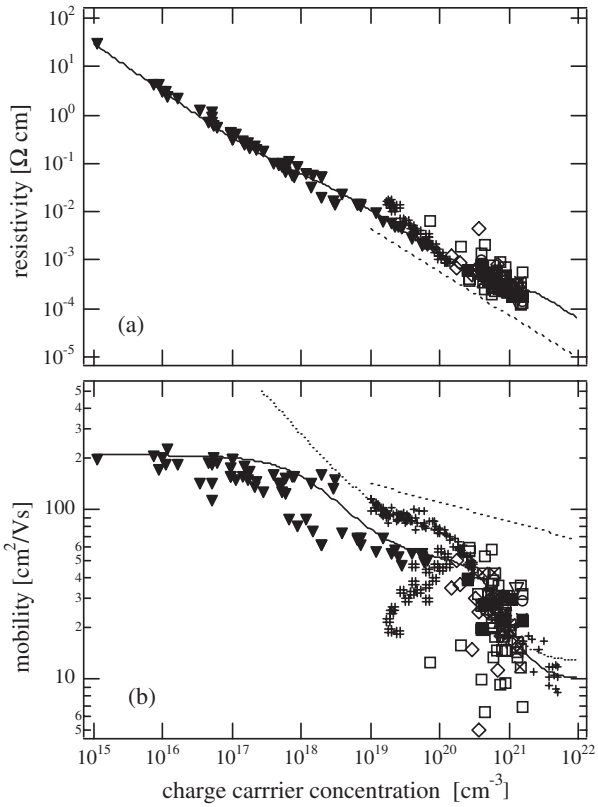

Figure 4. The resistivity (a) and Hall mobility (b) of doped and undoped single crystalline zinc oxide (▼) and zinc oxide films versus the charge carrier concentration. The meanings of the symbols for the ZnO films and the broken curves are explained in figures 1 and 3. For comparison, the mobility (+) of phosphorous-doped single crystalline silicon is added, together with an empirical fit curve (dotted curve) [24]. An analogous fit by the author for the ZnO data is displayed as a continuous curve (section 2.3).

investigated semiconductor today. Though the intrinsic room temperature mobility of n-type silicon (phosphorous-doped) is about 1400 cm^2 V^{-1} s^{-1} at low carrier concentrations [24], the mobilities for $n > 10^{20}$ cm^{-3} are comparable to that of polycrystalline ZnO films (see figure 4, crosses and dotted fit curve, equation (1)). Obviously, this is caused by the fact that for both semiconductors the same charge carrier scattering process—ionized impurity scattering—limits the mobility. It is remarkable that the mobility limit given by Bellingham *et al* [19] for TCO films is not even reached by heavily doped ($n > 10^{19}$ cm^{-3}) single crystalline silicon. The fact that the mobilities of single crystalline silicon and polycrystalline zinc oxide are in the same range for $n > 10^{19}$ cm^{-3} is a hint that the mobilities of heavily doped semiconductors are quite insensitive to the crystallographic quality and are governed by intrinsic material properties (see section 2.3).

Based on an empirical formula of Masetti *et al* [24]

$$\mu^{Ma} = \mu_{min} + \frac{\mu_{max} - \mu_{min}}{1 + (n/n_{ref1})^{\alpha_1}} - \frac{\mu_1}{1 + (n_{ref2}/n)^{\alpha_2}} \qquad (1)$$

the experimental data for ZnO have been fitted by the author (full curves in figures 4(b), 5 and 6). Despite the scattering of the ZnO data especially in the region around $n \approx 10^{18}$ cm^{-3} the fit equation (1), developed for silicon can be used also

Table 1. Fit parameters for silicon [24] and zinc oxide (Masetti's formula, equation (1)).

Fit parameter	Si (P)	Si (B)	ZnO
μ_{max} ($cm^2\ V^{-1}\ s^{-1}$) (lattice mobility)	1414	470.5	210
μ_{min} ($cm^2\ V^{-1}\ s^{-1}$) (ionized impurity mobility)	68.5	44.9	50
$\mu_{min} - \mu_1$ ($cm^2\ V^{-1}\ s^{-1}$) (clustering mobility)	12.4	15.9	10
n_{ref1} (cm^{-3})	9.2×10^{16}	2.23×10^{17}	2×10^{18}
α_1	0.711	0.719	1
n_{ref2} (cm^{-3})	3.41×10^{20}	6.1×10^{20}	6×10^{20}
α_2	1.98	2.0	2

for zinc oxide. Table 1 lists the fit parameters and their meaning for silicon [24] and zinc oxide. The ionized impurity mobility (μ_{min}) and the clustering mobility ($\mu_{min} - \mu_1$) are quite comparable for silicon and zinc oxide. This formula will be further discussed in section 2.3.

An observation of Bellingham *et al* [79], which they made for ITO films seems to be true for zinc oxide too. Taking arguments from the ionized impurity scattering theory (section 2.3) one would expect that doping by extrinsic dopants leads to higher mobilities by a factor of two compared to self doping due to oxygen vacancies, due to the different charge states of the ionized donors. However, this was not observed by Bellingham *et al* [79] for indium oxide films, doped by oxygen vacancies, and for tin-doped In_2O_3 films (ITO). The same can be seen by comparing the data of Minami *et al* [23] of self-doped (#) and aluminium-doped (⊠) zinc oxide films in figure 4(b). Both types of films exhibit about the same mobility of 50 $cm^2\ V^{-1}\ s^{-1}$ at a carrier concentration of $2 \times 10^{20}\ cm^{-3}$, though the theoretical mobilities should be different by a factor of two.

2.3. Carrier transport in zinc oxide films

In the well known reviews about TCO materials [18, 80–82] the carrier transport is treated in a very brief manner. Mostly it is only mentioned that the carrier transport is limited by ionized impurity scattering or by grain barriers. The recent review of Hartnagel *et al* [1] summarizes the different transport models, but without a detailed comparison of theory and experiment. In many papers [83] and textbooks [84] dealing with electrical properties of TCO films formulae are given for the mobilities, which are inadequate or wrong. Often the calculated mobilities are much higher than the measured ones: Shanthi *et al* [85] for instance calculated a mobility of 150 $cm^2\ V^{-1}\ s^{-1}$ using the Brooks–Herring formula. The overestimation of the mobility calculated by Bellingham *et al* [19] has been mentioned in section 2.2. The formulae for the ionized impurities limited mobility are given in many references only for singly ionized impurities, i.e. for a charge state $Z = 1$, which is a restriction for TCO materials, where impurities with $Z > 1$ are expected, for instance oxygen vacancies with $Z = 2$ (see [68]). For heavily doped TCO materials what Zawadzki [86] pointed out in his readable review article 'Classic transport effects are easy to measure and difficult to interpret' is valid. Therefore, in the following the analytical expressions for non-degenerate and degenerate semiconductors are summarized, based on the original papers and the reviews [86, 87].

For high charge carrier concentrations the mobility is determined by the scattering of the electrons at ionized impurities (intrinsic lattice defects or extrinsic dopants). The carrier transport in doped semiconductors was treated theoretically half a century ago, during the rise of semiconductor physics and technology after World War II. Conwell and Weisskopf [88, 89] were the first to derive a formula for the mobility μ_{ii} limited by ionized impurity scattering. They calculated the mobility in a non-degenerate semiconductor by treating the scattering process as uncorrelated collisions in a truncated Coulomb potential of ionized donors or acceptors. The Coulomb potential is cut off at half the mean distance $d = N_i^{-1/3}$ between two donors. Their expression for the mobility in SI units is [87]

$$\mu_{ii}^{CW} = \frac{128\sqrt{2\pi}(\varepsilon_r\varepsilon_0)^2(kT)^{3/2}}{\sqrt{m^*}Z^2e^3N_i} \times \left\{ \ln\left[1 + \left(\frac{12\pi\varepsilon_r\varepsilon_0 kT}{Ze^2N_i^{1/3}}\right)^2\right]\right\}^{-1}. \quad (2)$$

It can be seen that the mobility is determined by the material parameters: relative static permittivity ε_r; the effective mass m^*; and the charge Z of the impurity and its concentration N_i. The other symbols π, ε_0, e, k and T have their usual meaning. For a non-degenerate semiconductor the mobility exhibits a pronounced temperature dependence: $\mu_{ii} \sim T^{3/2}$, if the log-term is neglected.

The Z-dependence of μ_{ii} means that intrinsic doping by oxygen vacancies ($Z = 2$) should lead to a lower mobility (about a factor of two) than doping by extrinsic dopants like B, Al, In, Ga on the substitutional cation ($Z = 1$) or anion (F, Cl) lattice places. On the other hand, extrinsic dopants on interstitial places ($Z = 3$), which has been proposed recently as a doping mechanism in ZnO [90], should lead to even lower mobilities.

It was soon realized that the electron scattering in the Coulomb potential is too strong, yielding too low mobilities. Brooks [20, 91] and Herring (not published) calculated the mobility for a screened Coulomb potential, taking into account the screening of the ionized impurities by mobile charge carriers and obtained the expression:

$$\mu_{ii}^{BH} = \frac{128\sqrt{2\pi}(\varepsilon_r\varepsilon_0)^2(kT)^{3/2}}{\sqrt{m^*}Z^2e^3N_i}\frac{1}{F_{ii}(\xi)} \quad (3)$$

with

$$F_{ii}(\xi) = \ln(1+\xi) - \frac{\xi}{1+\xi}$$

and

$$\xi = \frac{96\pi^2\varepsilon_r\varepsilon_0 m^*}{N_i}\left(\frac{kT}{he}\right)^2 \quad (4)$$

which differs from the expression from Conwell and Weisskopf only by the screening function F_{ii}. The equations (2)–(4) are

valid for a non-degenerate electron gas, i.e. for n-type zinc oxide for $n < \approx 3.7 \times 10^{18}$ cm^{-3} at 300 K. This is clearly visible for the Brooks–Herring expression, which exhibits a pronounced, but unphysical minimum of the mobility around a carrier concentration of about 10^{19} cm^{-3} (see also Seeger [92]). Therefore, it is plausible, as already done by Brooks [20], to use only the logarithmic term in the screening function $F_{ii}(\xi)$, since in the non-degenerate region the condition $\xi \gg 1$ is fulfilled.

For high charge carrier concentrations (degenerate semiconductors) or low temperatures the expressions first derived by Shockley [93] for scattering at the truncated Coulomb potential and by Dingle [21] (see also [86]) for scattering at the screened Coulomb potential have to be used:

$$\mu_{ii}^{Sh} = \frac{3(\varepsilon_r\varepsilon_0)^2h^3}{Z^2m^{*2}e^3}\left\{\ln\left[1+\left(\frac{3^{2/3}\pi^{1/3}\varepsilon_r\varepsilon_0h^2n^{1/3}}{2m^*e^2}\right)^2\right]\right\}^{-1} \quad (5)$$

$$\mu_{ii}^{Di} = \frac{3(\varepsilon_r\varepsilon_0)^2h^3}{Z^2m^{*2}e^3}\frac{n}{N_i}\frac{1}{F_{ii}(\xi_d)} \quad (6)$$

with

$$\xi_d = (3\pi^2)^{1/3}\frac{\varepsilon_r\varepsilon_0h^2n^{1/3}}{m^*e^2} \quad (7)$$

where h is Planck's constant and n the electron density. The screening function F_{ii} is that of (4). Again, both expressions differ only in the screening terms for an uncompensated fully ionized semiconductor ($n = N_i$).

Johnson and Lark-Horowitz [94] derived an approximate expression for a degenerate electron gas that is often cited in papers and reviews about TCO materials [1, 23, 30, 83]. However, their derivation is valid only for carrier concentrations below about 10^{19} cm^{-3}, as pointed out by Shockley [93], a limitation neglected in the TCO literature. Due to this limitation this theory is not suited for highly doped semiconductors and is therefore not taken further into account. For a degenerate electron gas the mobility is independent of the temperature (see (5) and (6)), a property often used to characterize ionized impurity scattering.

The expressions derived by Brooks–Herring and by Dingle also take into account the case that not all impurities are ionized; therefore the charge carrier concentration n also occurs in formulae (6) and (7). If the semiconductor is (partly) compensated, instead of N_i the expressions $N_D + N_A$ and $n' = n + (n + N_A)[1 - (n + N_A)/N_D]$ have to be used in (6), where N_D, N_A are the donor and acceptor concentration, respectively.

The theoretical dependences for the screened Coulomb potential scattering (Brooks–Herring–Dingle) are compared with the experimental data in figure 5 (curves 1′ and 1). The calculations were performed for singly ionized impurities ($Z = 1$), if not otherwise stated. It was assumed that all impurities were ionized ($n = N_i$), an assumption, which is justified at room temperature. The transition region from the non-degenerate to the degenerate electron gas has not been smoothed. In order to obtain the total mobility μ a lattice mobility of the intrinsic zinc oxide of $\mu_{lat} \equiv \mu_{max} = 210$ cm^2 V^{-1} s^{-1} (see table 1) has been taken into account by Matthiessen's rule

$$\mu = \frac{\mu_{lat}\mu_{ii}}{\mu_{lat} + \mu_{ii}}. \quad (8)$$

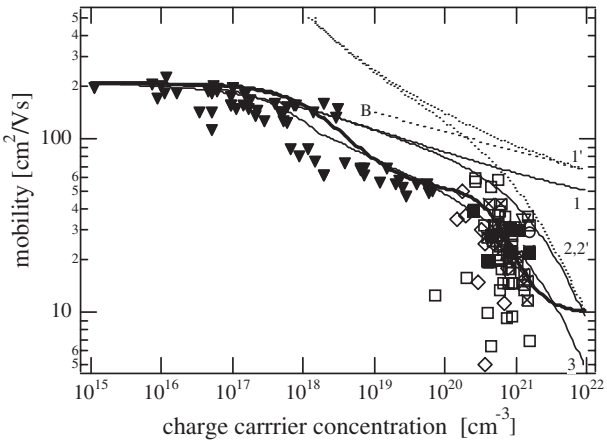

Figure 5. The Hall mobility of undoped and doped ZnO single crystals and films versus the charge carrier concentration. The analytical theoretical mobilities (see section 2.3) are shown as thin dotted (ionized impurity mobility, μ_{ii}—1′, 2′) and full (total mobility, μ—1, 2, 3) curves. 1, theory of Brooks–Herring–Dingle (parabolic band); 2, theory of Brooks–Herring–Dingle (non-parabolic band); 3, theory of Brooks–Herring–Dingle (non-parabolic band, oxygen vacancies as dopants, i.e. $Z = 2$); B is the estimation of Bellingham *et al* [19].

Due to the relatively low value of the lattice mobility in zinc oxide, the total mobility is significantly influenced by μ_{lat}, especially in the region $10^{19} < n < 10^{20}$ cm^{-3}, a fact, often ignored by other authors [23, 83]. The Brooks–Herring–Dingle theory for the screened Coulomb potential yields mobilities which are too high by a factor of about two. This is in remarkable agreement with the recent theory of Schenk [9] for the mobility of doped silicon, who found a factor of 2.2. The physically more doubtful theory for the truncated Coulomb potential (Conwell–Weisskopf–Shockley) gives better agreement (not shown in figure 5) with the experimental ZnO data, which seems to be caused by chance.

In a first approximation the material parameters, effective mass and dielectric constant, determine the absolute value of the ionized impurity scattering mobility. These parameters are not very different for zinc oxide and silicon, as can be seen from table 2, where the different properties of zinc oxide and other TCO materials are compared with the corresponding parameters of silicon. Therefore, the fact, that heavily doped single crystalline silicon exhibits quite similar Hall mobilities as heavily doped zinc oxide films can be explained by the 'classical' theory. Taking only the prefactor of (5) or (6), μ_{ii} is proportional to $(\varepsilon_r/m^*)^2$, yielding a ratio $\mu_{ii}(\mathrm{Si})/\mu_{ii}(\mathrm{ZnO}) = 1.39$ (constants taken from table 2), which is quite well reproduced by the ratio $\mu_{min}(\mathrm{Si})/\mu_{min}(\mathrm{ZnO}) = 1.37$ (values taken from table 1), where μ_{min} is the mobility limit due to ionized impurity scattering.

For $n > 10^{20}$ cm^{-3} the theoretical dependence of the mobility (parabolic band structure) on the charge carrier concentration is rather weak. A numerical fit in the region $10^{19} < n < 10^{21}$ cm^{-3} gives a power law dependence of $\mu_{total} \sim n^{-1/5.6}$ (see curve 1 in figure 5), which is different from the often cited exponents (-1 or $-2/3$). This is due to the fact, that the logarithmic terms are neglected and the relatively low lattice mobility of $\mu_{lat} \approx 210$ cm^2 V^{-1} s^{-1} has to be taken into account by applying Matthiesen's rule. In

Table 2. Properties of zinc oxide and other TCO-materials in comparison to that of silicon [82, 84, 100].

Property	In_2O_3	SnO_2	ZnO	Si [84]
Mineral name	—	cassiterite	zincite	silicon
Average amount of the metal in the earth's crust (ppm)	0.1	40	132	2.58×10^5
Band gap E_g (300 K) (eV)	2.7 (indir) 3.75 (dir)	3.6 (dir)	3.4 (dir)	1.12 (indir) 4.18 (dir)
Pressure coefficient dE_g/dp (meV kbar^{-1})			2.33	−1.41
Static dielectric constant ε_r	≈9	$\|c$: 9.6 $\perp c$: 13.5	$\|c$: 8.75 $\perp c$: 7.8	11.9
Effective electron mass m^*/m_e	0.35	$\|c$: 0.23 $\perp c$: 0.3	0.28	0.337
Non-parabolicity parameter α (eV^{-1})		0.96 [97]	0.29 1.04 [23]	0.27 [101] 0.5 [9]
Effective conduction band density of states (300 K) N_C (cm^{-3})	4.1×10^{18}	3.7×10^{18}	3.7×10^{18}	4.9×10^{18}
Extrinsic dopants	Sn, Ti, Zr, F, Cl, Sb, Ge, Zn, Pb, Si	Sb, (As, P) F, Cl	B, Al, Ga, In, Si, Ge, Sn, Y, Sc, Ti, Zr, Hf F, Cl	B, Al, Ga, In P, As, Sb
Other phases in the dopant–host system (heat of formation (eV))	$In_4Sn_3O_{12}$ SnO (2.9) SnO_2 (6.0) TiO_2 (9.8) ZrO_2 (11.2) GeO_2 (5.6) SiO_2 (8.8) ZnO (3.6) Sb_2O_3 (7.2) Sb_2O_5 (10.0)	As_2O_3 (6.7) As_2O_5 (9.5) Sb_2O_3 (7.2) Sb_2O_5 (10.0) P_2O_5 (15.6)	ZnO_2 B_2O_3 (6.6) Al_2O_3 (8.7) Ga_2O_3 (5.7) In_2O_3 (4.8) TiO_2 (9.8) Y_2O_3 (19.8) HfO_2 (11.8) ZrO_2 (11.2) $ZnAl_2O_4$ (21.4) $ZnGa_2O_4$ (15.3)	SiB_3 SiB_6 SiP SiAs $SiAs_2$
Crystal structure	cubic, bixbyite	tetragonal, rutile	hexagonal, wurtzite	cubic, diamond
Space group (number)	$I2_13$ (no199)	$P4_2mnm$ (no 136)	$P6_3mc$ (no 186)	Fd3m (no 227)
Lattice parameter(s) (nm)	a: 1.012	a: 0.474 c: 0.319	a: 0.325 c: 0.5207	a: 0.5431
Density ρ (g cm^{-3})	7.12	6.99	5.67	2.33
Thermal expansion α (300 K) (10^{-6} K^{-1})	6.7	$\|c$: 3.7 $\perp c$: 4.0	$\|c$: 2.92 $\perp c$: 4.75	2.59
Melting point (°C)	2190	>1900[a]	2240	1415
Melting point of the metal (°C)	157	232	420	1415
Heat of formation (eV)	9.7	6.0	3.6	—

[a]Decomposition into SnO and O_2 at 1500 °C.

other words, an experimentally found dependence $\mu \sim n^{-1}$ or $n^{-2/3}$ (see [23, 95]) is not an indication of ionized impurity scattering.

The significant differences between theory and experiment in the region of degeneracy have led to improvements of the theory of ionized impurity scattering by taking into account the non-parabolicity of the conduction band [96]. Zawadzki [86] calculated an analytical expression for the screening function F_{ii}^{np} for the case of a non-parabolic band structure which was further simplified by Pisarkiewicz *et al* [97]

$$F_{ii}^{np} = \left[1 + \frac{4\xi_{np}}{\xi}\left(1 - \frac{\xi_{np}}{8}\right)\right]\ln(1+\xi) - \frac{\xi}{1+\xi} - 2\xi_{np}\left(1 - \frac{5\xi_{np}}{16}\right) \quad (9)$$

with the additional parameter

$$\xi_{np} = 1 - \frac{m_0^*}{m^*} \quad (10)$$

which describes the non-parabolicity of the conduction band, with m_0^*, the effective mass at the conduction band edge. For a parabolic band ($m^* = m_0^*$) $\xi_{np} = 0$, and (9) reduces to the expression (4). The dependence of the effective mass on the electron energy in the conduction band was approximated by [86]

$$m^* = m_0^*[1 + 2\alpha(E - E_C)]. \quad (11)$$

Here, α is the non-parabolicity parameter (see table 2), $E - E_C$ the electron energy relative to the conduction band edge E_C [97]. Though experimental data on the effective mass of ZnO versus electron density are rare in literature, this approximation seems to be applicable to zinc oxide. Brehme *et al* [51] reported for Al-doped ZnO an effective mass of $m^* = 0.5m_e$ in the region $n > 10^{20}$ cm^{-3}, which is compatible with a non-parabolicity parameter of $\alpha = 0.29$ eV^{-1}, corresponding to the rule $\alpha \approx 1/E_g$ (E_g is the band gap energy) [86]. Using the approximation for the relation between the reduced Fermi energy $\eta = (E_F - E_C)/kT$ and the Fermi–Dirac integral $F_{1/2}(\eta) = n/N_C$, given by Nilsson [98] (see also [99]), an

analytical equation for the dependence of m^* on the electron density n can be written as

$$\frac{m^*}{m_0^*} = 1 + 2\alpha kT\left(\frac{\ln(n/N_C)}{1-(n/N_C)^2} + \frac{(3\sqrt{\pi}(n/4N_C)^{2/3})}{1+[0.24+1.08(3\sqrt{\pi}(n/4N_C)^{2/3})]^{-2}}\right). \quad (12)$$

From (2)–(12) the theoretical mobilities for a non-parabolic conduction band have been calculated, which also are shown in figure 5 (curves 2′, 2, 3). The inclusion of the non-parabolicity of the conduction band reduces μ_{ii} for $n > 10^{20}$ cm^{-3}. However, the improvement towards the experimental data is not sufficient for a satisfying agreement. The best overall agreement has been achieved by setting $Z = 2$, which corresponds to doping by oxygen vacancies. Together with the fact that oxygen vacancy doping and extrinsic doping lead to the same mobilities (see section 2.2), this could be an indication that the true doping mechanism is due to oxygen vacancies in both cases. In this line of argument extrinsic doping would generate oxygen vacancies due to the formation of the corresponding extrinsic dopant oxide (for instance B_2O_3, Al_2O_3, Ga_2O_3). This is supported by the fact that the oxide forming elements Hf, Ti, Y, Zr can also be used to dope zinc oxide [11].

However, the scattering of the data, both for single crystals and polycrystalline films is too high, in order to definitely decide between these two charge states. On the other hand, for highly doped silicon a better agreement is also reached by setting $Z = 2$, which, however, is not plausible for dopants such as phosphorous or arsenic. That means there seems to be a principal discrepancy between theory and experiment. Recently, Minami and co-workers [11, 23] used Dingle's theory with the non-parabolic band structure of ZnO in order to fit their data, which were also used in this paper. However, their non-parabolicity constant of $\alpha = 1.04$ eV^{-1} leads to an effective mass at a carrier concentration of 1×10^{21} cm^{-3} of $m^* = 1.04\ m_e$, which seems to be too high (see Brehme *et al* [51]).

Another observation can be made by comparing the mobilities of silicon and zinc oxide in the region $n > 10^{20}$ cm^{-3} (figure 6); for heavily doped silicon (both n- and p-type) a significant decrease of the mobility, i.e. a higher scattering, is observed for carrier concentrations $>5 \times 10^{20}$ cm^{-3}, which cannot be explained by the 'classical' theories of ionized impurity scattering. Also a recent analytical theoretical treatment of Schenk [9] of the mobility in silicon, taking into account the non-parabolic and anisotropic band structure of silicon as well as the dispersive screening and the perturbation of the density of states of the conduction band edge at carrier concentrations $n > 10^{20}$ cm^{-3} [9] was not able to describe the experimental data in this region very well. Furthermore, for $10^{16} < n < 10^{19}$ cm^{-3}, the agreement between his theory and the experimental data is not good. Eventually the author uses a scaling factor of 2.2 for the Brooks–Herring theory in order to fit his too high theoretical data to the experiment. Schenk suggests that major contributions to this factor arise from electron–electron (e–e) scattering and from electron–plasma interaction [102].

In order to explain the mobilities in their heavily doped germanium samples in the ionized impurity scattering region,

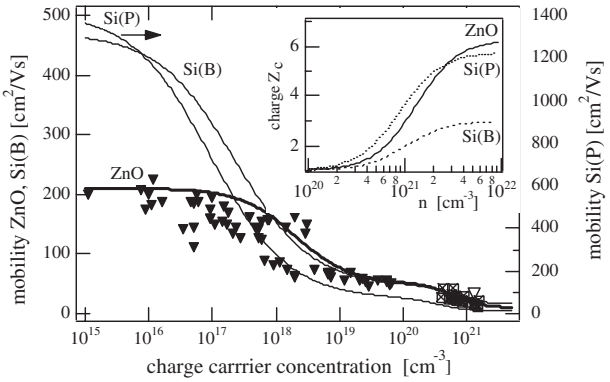

Figure 6. The dependence of the Hall mobility of undoped and doped ZnO single crystals and films on the charge carrier concentration. For comparison the corresponding dependences of boron and phosphorous doped single crystalline silicon (numerical fits of Masetti *et al* [24]) are included. For zinc oxide a fit curve based on the analytical fit expression of Masetti *et al* is given too. The inset shows the cluster functions of Si(P) (dotted), Si(B) (dashed) according to Klaassen [25] and of ZnO (this work).

Dakhovskii *et al* [103] introduced in 1971 the plausible statistical argument of impurity clustering. Clusters of impurities act as scattering centres with a charge Z_C which leads to a higher scattering due to the Z^{-2}-dependence of the mobility on the charge (see (2), (3) and (5)). This argument has found little interest in theories of ionized impurity scattering. Recently, Klaassen [8] took up this idea of an additional scattering process by ionized impurity clusters in order to describe the mobility in silicon, heavily doped with boron, arsenic or phosphorous. Based on the empirical formula of Masetti *et al* [24] (see (1)) Klaassen calculated the cluster charge Z_C as a function of the charge carrier concentration, shown as an inset in figure 6. The fit parameters of (1) have the following meaning: μ_{max} and μ_{min} can be identified as the lattice mobility at low and the ionized impurity limited mobility at high carrier concentrations. $\mu_{min} - \mu_1$ is the mobility limit caused by the process of scattering at ionized impurity clusters. The parameters $n_{ref\ 1}$, $n_{ref\ 2}$, α_1 and α_2 describe the transitions (location and steepness) from the lattice to the ionized impurity scattering and to the cluster scattering. According to this semiempirical fit phosphorous-doped silicon forms ionized impurity clusters up to $Z_C = 6$, while boron-doped silicon exhibits clusters up to $Z_C = 3$ (see figure 6). It is quite plausible from these statistical arguments, that such a clustering process is also acting in the case of zinc oxide (or other TCO materials). With the formula of Masetti *et al* [24], the dependence of the electron mobility on the carrier concentration in zinc oxide was fitted. Due to the limited data for single crystalline zinc oxide (c-ZnO) and due to the large scattering of the data for polycrystalline ZnO films, the fit was performed with a selected data set consisting of the c-ZnO values for $n < 10^{20}$ cm^{-3} and the consistent data set for polycrystalline doped zinc oxide films of Minami *et al* [23] for $n > 4 \times 10^{20}$ cm^{-3}. The fitted mobility curve is shown in figures 4(b)–6 as full curves. It is interesting to note that the values of the cluster limited mobility $\mu_{min} - \mu_1$ are quite similar for silicon and zinc oxide (see table 1). By applying the cluster model to the ZnO fit curve the cluster size curve of ZnO shown in the inset of figure 6 was obtained. The overall

shape of this curve is quite comparable to P-doped silicon with a maximum cluster size of $Z_C \approx 6$.

There are a lot of other theoretical approaches (for a review see [9] or [87]) that include higher order effects to describe the mobility of doped semiconductors:

- electron–electron scattering [96, 104, 105];
- refinement of the Born approximation for the scattering cross section [22, 106];
- dispersive screening [9, 107];
- perturbed band edge structure due to dopants [9];
- electron–plasma interaction [102].

The electron–electron scattering correction, which is important only in the non-degenerate region (i.e. below about 1×10^{20} cm^{-3}) amounts to a maximum reduction of μ_{ii} by a factor of about 0.6 [96, 104]. It has been checked that the influence on the total mobility in ZnO is negligible due to the low lattice mobility of this material.

The other theoretical refinements have not been applied to the ZnO mobility data, since the scattering of the experimental data is still too high in order to prove these models for zinc oxide.

3. Conclusions

The electrical parameters of single crystalline zinc oxide and of polycrystalline films have been reviewed. The lowest resistivities reported are in the range of 1.4 to 2×10^{-4} Ω cm, independently of the deposition method. The scattering of the data—both for single crystalline and polycrystalline ZnO—is high, illuminating the fact that zinc oxide is not as well investigated and developed as other semiconductors, especially silicon. The electrical parameters do not show a pronounced dependence on deposition parameters (temperature and pressure) for magnetron-sputtered films, which is argued to be due to differences in the magnetron sputtering arrangements (type of the magnetron, target-to-substrate distance, ion bombardment of the growing film). When viewing the electrical parameters over the time it can be seen that the lowest resistivities and the highest mobilities have not changed in the last 15 years, despite a lot of technological effort in this period.

Analytical theoretical expressions for the ionized impurity limited mobility have been reviewed in this paper too and compared to the experimental mobilities of single and polycrystalline ZnO. It is found that the mobility according to the theory of Brooks, Herring and Dingle gives too high mobilities in the region $n > 10^{20}$ cm^{-3}, if a charge state of the donors of $Z = 1$ is used. The inclusion of the non-parabolic band structure reduces the theoretical mobilities in the degenerate region and improves the agreement with the experiment.

Another scattering mechanism due to impurity clusters as suggested recently by Klaassen for heavily doped silicon, seems also to act in zinc oxide, especially for very high carrier concentrations $n > 5 \times 10^{20}$ cm^{-3}. Due to statistical reasons such an effect is independent of the specific material and therefore also plausible for zinc oxide and other TCO materials.

Taking an ionized donor charge state of $Z = 2$, as supposed for oxygen vacancies, the calculated mobility decreases by a factor of two, which leads to a rather good agreement with the experimental data. However, the scattering of the experimental mobility values is too high to exactly determine the donors charge state.

Taking all the results together:

- an upper limit of the carrier concentration of about 1.5×10^{21} cm^{-3} (which corresponds to a dopant solubility limit of about 4 at%);
- an upper limit of the carrier mobility in the region $n > 5 \times 10^{20}$ cm^{-3} of about 40 cm^2 V^{-1} s^{-1},

it seems reasonable to suppose, that resistivities less than 1×10^{-4} Ω cm for doped polycrystalline zinc oxide films are hard to achieve, due to a general limitation by ionized impurity scattering. This assumption is further supported by the fact that heavily n-doped single crystalline silicon also exhibits mobilities in the same range as polycrystalline ZnO films. The arguments given above for zinc oxide apply equally well to the other TCO materials, tin oxide and indium–tin oxide (ITO), see figure 1 in the recent review of Minami [11].

Concerning the carrier concentration a second argument leads to a practical upper limit of about 1.5×10^{21} cm^{-3}. With increasing carrier concentration the absorption edge due to free carriers shifts towards the visible range. Therefore, the intended application as transparent window layers in the visible sets the same upper limit of n as the limited dopant solubility.

4. Outlook

Electrical transport investigations of heavily doped zinc oxide single crystals and/or epitaxial films should be performed in order to obtain further insight into the charge carrier transport mechanisms such as:

- charge state of the donors in intrinsically and extrinsically doped ZnO;
- dopant clustering;
- band structure of the conduction band of heavily doped zinc oxide;
- formation of secondary (for instance Al_2O_3) and ternary (for instance gahnite, $ZnAl_2O_4$) phases in ZnO and its relation to doping.

The suggested limitation of the mobility by ionized impurity scattering is valid only for homogeneously doped films. The mobility in semiconductors can be increased by the so-called modulation doping method, introduced by Dingle *et al* [108] for GaAs–Al_x/Ga_{1-x}As superlattice structures (see also [109]). The principle of modulation doping consists in stacking lowly and heavily doped films with slightly different bandgaps. While the heavily doped films spend the charge carriers their transport occurs in the lowly doped layers of the stack which are not subjected to the ionized impurity scattering limitation of the mobility. Recently, Rauf [110] reported very high mobilities in ITO films which he claimed to be due to the modulation doping effect. However, in his case the highly and lowly doped regions were laterally arranged in the films and not vertically, as in true superlattice structures.

Nevertheless, it appears to be promising to try the modulation doping of zinc oxide and other TCO materials in order to overcome the inherent mobility limitation due to ionized impurity scattering.

Acknowledgment

B Selle is gratefully acknowledged for fruitful discussions and careful reading of the manuscript.

References

[1] Hartnagel H L, Dawar A L, Jain A K and Jagadish C 1995 *Semiconducting Transparent Thin Films* (Bristol: Institute of Physics Publishing)
[2] Minami T, Sato H, Nanto H and Takata S 1989 *Thin Solid Films* **171** 277
[3] Beneking C, Rech B, Wieder S, Kluth O, Wagner H, Frammelsberger W, Geyer R, Lechner P, Rübel H and Schade H 1999 *Thin Solid Films* **351** 241
[4] Look D C, Reynolds D C, Sizelove J R, Jones R L, Litton C W, Cantwell G and Harsch W C 1998 *Solid State Commun.* **105** 399
[5] Iwata K, Fons P, Yamada A, Matsubara K and Niki S 2000 *J. Cryst. Growth* **209** 526
[6] Ryu Y R, Zhu S, Look D C, Wrobel J M, Jeong H M and White H W 2000 *J. Cryst. Growth* **216** 330
[7] Look D C, Hemsky J W and Sizelove J R 1999 *Phys. Rev. Lett.* **82** 2552
[8] Klaassen D B M 1992 *Solid-State Electron.* **35** 961
[9] Schenk A 1996 *J. Appl. Phys.* **79** 814
[10] Wu X, Coutts T J and Mulligan W P 1997 *J. Vac. Sci. Technol.* A **15** 1057
[11] Minami T 2000 *MRS Bull.* **25** 38
[12] Freeman A J, Poeppelmeier K R, Mason T O, Chang R P H and Marks T J 2000 *MRS Bull.* **45**
[13] Blom F R, Pol F C M v d, Bauhuis G and Popma T J A 1991 *Thin Solid Films* **204** 365
[14] Ziegler E, Heinrich A, Oppermann H and Stöver G 1981 *Phys. Status Solidi* a **66** 635
[15] Kobiakov I B 1980 *Solid State Commun.* **35** 305
[16] Caporaletti O 1982 *Solar Energy Mater.* **7** 65
[17] Sieber I, Wanderka N, Urban I, Dörfel I, Schierhorn E, Fenske F and Fuhs W 1998 *Thin Solid Films* **330** 108
[18] Chopra K L, Major S and Pandya D K 1983 *Thin Solid Films* **102** 1
[19] Bellingham J R, Phillips W A and Adkins C J 1992 *J. Mater. Sci. Lett.* **11** 263
[20] Brooks H 1955 *Adv. Electr. Electron Phys.* **7** 85
[21] Dingle R B *Phil. Mag.* **46** 831
[22] Moore E J 1967 *Phys. Rev.* **160** 618
[23] Minami T, Sato H, Ohashi K, Tomofuji T and Takata S 1992 *J. Cryst. Growth* **117** 370
[24] Masetti G, Severi M and Solmi S 1983 *IEEE Trans. Electron Dev.* **ED30** 764
[25] Klaassen D B M 1992 *Solid-State Electron.* **35** 953
[26] Powell R A and Rossnagel S M 1999 *Thin Films. PVD for Microelectronics: Sputter Deposition Applied to Semiconductor Manufacturing* (San Diego, CA: Academic) p 1
[27] Ellmer K 2000 *J. Phys. D: Appl. Phys.* **33** R17
[28] Webb J B, Williams D F and Buchanan M 1981 *Appl. Phys. Lett.* **39** 640
[29] Minami T, Nanto H and Takata S 1985 *Thin Solid Films* **124** 43
[30] Minami T, Sato H, Nanto H and Takata S 1985 *Japan. J. Appl. Phys.* **24** L781
[31] Qiu S N, Qiu C X and Shih I 1987 *Solar Energy Mater.* **15** 261
[32] Jin Z-C, Hamberg I and Granqvist C G 1988 *J. Appl. Phys.* **64** 5117
[33] Choi B H, Im H B, Song J S and Yoon K H 1990 *Thin Solid Films* **193/194** 712
[34] Harding G L, Window B and Horrigan E C 1991 *Solar Energy Mater.* **22** 69
[35] Sato H, Minami T, Takata S, Mouri T and Ogawa N 1992 *Thin Solid Films* **220** 327
[36] Mauch R H and Schock H W 1991 *Proc. 10th Eur. Photovoltaic Solar Energy Conf. (Lisbon, Portugal)* (Dordrecht: Kluwer) p 88
[37] Konishi R, Noda K, Harada H and Sasakura H 1992 *J. Cryst. Growth* **117** 939
[38] Schäffler R and Schock H W 1993 *Proc. 23rd IEEE Photovoltaic Specialists Conf. (Louisville, Kentucky, 10–14 May 1993)* p 1026
[39] Martinez M A, Herrero J and Gutierrez M T 1994 *Proc. 12th Eur. Photovoltaic Solar Energy Conf. (Amsterdam, The Netherlands, 11–15 April)* (Bedford: Stephens) p 1503
[40] Nakada T, Murakami N and Kunioka A 1994 *Proc. 12th Eur. Photovoltaic Solar Energy Conf. (Amsterdam, Netherlands, 11–15 April)* (Bedford: Stephens) p 1507
[41] Tominaga K, Kataoka M, Ueda T, Chong M, Shintani Y and Mori I 1994 *Thin Solid Films* **253** 9
[42] Kim K H, Park K C and Ma D Y 1997 *J. Appl. Phys.* **81** 7764
[43] Tominaga K, Manabe H, Umezu N, Mori I, Ushiro T and Nakabayashi I 1997 *J. Vac. Sci. Technol.* A **15** 1074
[44] Kluth O, Rech B, Houben L, Wieder S, Schöpke G, Beneking C, Wagner H, Löffl A and Schock H W 1999 *Thin Solid Films* **351** 247
[45] Löffl A, Wieder S, Rech B, Kluth O, Beneking C and Wagner H 1997 *Proc. 14th Eur. Photovoltaic Solar Energy Conf. (Barcelona, Spain, 30 June–4 July)* (Bedford: Stephens) p 2089
[46] Park K C, Ma D Y and Kim K H 1997 *Thin Solid Films* **305** 201
[47] Cebulla R, Wendt R and Ellmer K 1998 *J. Appl. Phys.* **83** 1087
[48] Menner R, Schäffler R, Sprecher B and Dimmler B 1998 *Proc. 2nd World Conf. Exhib. Photovoltaic Solar Energy Conf. (Vienna, 6–10 July 1998)* p 660
[49] Jäger S, Szyszka B, Szczyrbowski J and Bräuer G 1998 *Surf. Coat. Technol.* **98** 1304
[50] Fukawa M, Miyazaki M, Mitsui A and Sato K 1999 *Proc. Int. Workshop Optoelectronic Oxides: Material and Processing (Tokyo 1999)* p 81
[51] Brehme S, Fenske F, Fuhs W, Neubauer E, Poschenrieder M, Selle B and Sieber I 1999 *Thin Solid Films* **342** 167
[52] Hu J and Gordon R G 1991 *Solar Cells* **30** 437
[53] Yamada A, Wenas W W, Yoshino M, Konagai M and Takahashi K 1991 *Japan. J. Appl. Phys.* **30** L1152
[54] Hu J and Gordon R G 1992 *J. Appl. Phys.* **71** 880
[55] Hu J and Gordon R G 1992 *Proc. Mater. Res. Soc. Symp.* p 743
[56] Sato H, Minami T, Miyata T, Takata S and Ishii M 1994 *Thin Solid Films* **246** 65
[57] Lujala V, Skarp J, Tammenmaa M and Suntola T 1994 *Appl. Surf. Sci.* **82/83** 34
[58] Ataev B M, Bagamadova A M, Djabrailov A M, Mamedov V V and Rabadanov R A 1995 *Thin Solid Films* **260** 19
[59] Saito K, Watanabe Y, Takahashi K, Matsuzawa T, Sang B and Konagai M 1997 *Solar Energy Mater. Solar Cells* **49** 187
[60] Suzuki A, Matsushita T, Wada N, Sakamoto Y and Okuda M 1996 *Japan. J. Appl. Phys.* **35** L56
[61] Naghavi N, Rougier A, Marcel C, Guery C, Leriche J B and Tarascon J M 2000 *Thin Solid Films* **360** 233
[62] Rupprecht H 1958 *J. Phys. Chem. Solids* **6** 144
[63] Igasaki Y and Saito H 1991 *J. Appl. Phys.* **70** 3613
[64] Minami T, Sato H, Imamoto H and Takata S 1992 *Japan. J. Appl. Phys.* **31** L257
[65] Tominaga K, Yuasa T, Kume M and Tada O 1985 *Japan. J. Appl. Phys.* **24** 944
[66] Tominaga K, Iwamura S, Fujita I, Shintani Y and Tada O 1982 *Japan. J. Appl. Phys.* **21** 999
[67] Greene J E, Barnett S A, Sundgren J-E and Rockett A 1989 *Ion Beam Assisted Film Growth* ed T Itoh (Amsterdam: Elsevier) p 101
[68] Frank G and Köstlin H 1982 *Appl. Phys.* A **27** 197

[69] Einspruch G 1985 *VLSI Handbook* (New York: Academic) p 241
[70] Hutson A R 1959 *J. Phys. Chem. Solids* **8** 467
[71] Hausmann A and Teuerle W 1972 *Z. Phys.* **257** 299
[72] Wagner P and Helbig R 1974 *J. Phys. Chem. Solids* **35** 327
[73] Utsch B and Hausmann A 1975 *Z. Phys.* B **21** 27
[74] Ziegler E, Heinrich A, Oppermann H and Stöver G 1982 *Phys. Status Solidi* a **70** 563
[75] Venger E F, Melnichuk A V, Melnichuk L Y and Pasechnik Y A 1995 *Phys. Status Solidi* b **188** 823
[76] Seto J Y 1975 *J. Appl. Phys.* **46** 5247
[77] Bruneaux J, Cachet H, Froment M and Messad A 1991 *Thin Solid Films* **197** 129
[78] Hagemark K I and Chacka L C 1975 *J. Solid State Chem.* **15** 261
[79] Bellingham J R, Phillips W A and Adkins C J 1990 *J. Phys.: Condens. Matter* **2** 6207
[80] Vossen J L 1977 *Physics of Thin Films* ed G Hass, M H Francombe and R W Hoffmann (New York: Academic) p 1
[81] Dawar A L and Joshi J C 1984 *J. Mater. Sci.* **19** 1
[82] Szyszka B 2001 *Vakuum Forschung Praxis* **13** 38
[83] Kulkarni A K and Knickerbocker S A 1996 *J. Vac. Sci. Technol.* A **14** 1709
[84] Böer K W 1990 *Survey of Semiconductor Physics. Electrons and Other Particles in Bulk Semiconductors* (New York: Van Nostrand Reinhold) p 795
[85] Shanthi E, Banerjee A, Dutta V and Chopra K L 1980 *J. Appl. Phys.* **51** 6243
[86] Zawadzki W 1982 *Handbook on Semiconductors* ed T S Moss (Amsterdam: North-Holland) p 713
[87] Chattopadhyay D and Queisser H J 1981 *Rev. Mod. Phys.* **53** 745
[88] Conwell E and Weisskopf V F 1946 *Phys. Rev.* **69** 258
[89] Conwell E and Weisskopf V F 1950 *Phys. Rev.* **77** 388
[90] Wang R, Sleight A W and Cleary D 1996 *Chem. Mater.* **8** 433
[91] Brooks H 1951 *Phys. Rev.* **83** 879
[92] Seeger K 1991 *Semiconductor Physics* (Berlin: Springer) p 163
[93] Shockley W 1950 *Electrons and Holes in Semiconductors* (Toronto: van Nostrand) p 280
[94] Johnson V A and Lark-Horovitz K 1947 *Phys. Rev.* **71** 374
[95] Noguchi S and Sakata H 1980 *J. Phys. D: Appl. Phys.* **13** 1129
[96] Bate R T, Baxter R D, Reid F J and Beer A C 1965 *J. Phys. Chem. Solids* **26** 1205
[97] Pisarkiewicz T, Zakrzewska K and Leja E 1989 *Thin Solid Films* **174** 217
[98] Nilsson N G 1973 *Phys. Status Solidi* a **19** K75
[99] Blakemore J S 1982 *Solid-State Electron.* **25** 1067
[100] Madelung O 1996 *Semiconductors—Basic Data* (Berlin: Springer) p 317
[101] Dargys A and Kundrotas J 1994 *Handbook of Physical Properties of Ge, Si, GaAs and InP* (Vilnius: Science and Encyclopedia) p 123
[102] Fischetti M V 1991 *Phys. Rev.* B **44** 5527
[103] Dakhovskii I V, Polyanskaya T A, Samoilovich A G and Shartsev Y V 1971 *Sov. Phys.–Semicond.* **4** 1857
[104] Appel J 1961 *Phys. Rev.* **122** 1760
[105] Luong M and Shaw A W 1971 *Phys. Rev.* B **4** 2436
[106] Moore E J 1967 *Phys. Rev.* **160** 607
[107] Takimoto N 1959 *J. Phys. Soc. Japan* **14** 1142
[108] Dingle R, Störmer H-L, Gossard A C and Wiegmann W 1978 *Appl. Phys. Lett.* **33** 665
[109] Harris J J, Pals J A and Woltjer R 1989 *Rep. Progr. Phys.* **52** 1217
[110] Rauf I A 1993 Mater. Lett. **18** 123